This article is published as part of the *Dalton Transactions* themed issue entitled:

Radiopharmaceuticals for Imaging and Therapy

Guest Editors Stephen Faulkner (Oxford University) and Nick Long (Imperial College)

Published in issue 23, 2011 of *Dalton Transactions*

Image reproduced with permission of Martin W. Brechbiel

Articles in the issue include:

PERSPECTIVES:

ARTICLES:

Visit the *Dalton Transactions* website for more cutting-edge inorganic, organometallic and bioinorganic research
www.rsc.org/dalton

Dalton Transactions

Dynamic Article Links

Cite this: *Dalton Trans.*, 2011, **40**, 6278

www.rsc.org/dalton

PAPER

Investigating the binding properties of porous drug delivery systems using nuclear sensors (radiotracers) and positron annihilation lifetime spectroscopy—Predicting conditions for optimum performance

Eskender Mume,[a,b] Daniel E. Lynch,[c] Akira Uedono[d] and Suzanne V. Smith*[a]

Received 1st November 2010, Accepted 25th January 2011
DOI: 10.1039/c0dt01499k

Understanding how the size, charge and number of available pores in porous material influences the uptake and release properties is important for optimising their design and ultimately their application. Unfortunately there are no standard methods for screening porous materials in solution and therefore formulations must be developed for each encapsulated agent. This study investigates the potential of a library of radiotracers (nuclear sensors) for assessing the binding properties of hollow silica shell materials. Uptake and release of Cu^{2+} and Co^{2+} and their respective complexes with polyazacarboxylate macrocycles (dota and teta) and a series of hexa aza cages (diamsar, sarar and bis-(*p*-aminobenzyl)-diamsar) from the hollow silica shells was monitored using their radioisotopic analogues. Coordination chemistry of the metal (**M**) species, subtle alterations in the molecular architecture of ligands (**Ligand**) and their resultant complexes (**M-Ligand**) were found to significantly influence their uptake over pH 3 to 9 at room temperature. Positively charged species were selectively and rapidly (within 10 min) absorbed at pH 7 to 9. Negatively charged species were preferentially absorbed at low pH (3 to 5). Rates of release varied for each nuclear sensor, and time to establish equilibrium varied from minutes to days. The subtle changes in design of the nuclear sensors proved to be a valuable tool for determining the binding properties of porous materials. The data support the development of a library of nuclear sensors for screening porous materials for use in optimising the design of porous materials and the potential of nuclear sensors for high through-put screening of materials.

Introduction

Significant progress in the fabrication of supramolecular objects with novel phase morphologies, architectures and functions has been achieved in recent times.[1–6] Of particular importance are the hollow spherical aggregates, which have potential for encapsulating cargo molecules within the "empty" core domains.[7,8] Breakthrough in the synthesis of mesoporous silica materials with controlled particle size, morphology and porosity has enabled new applications in medicine, environment and industry.[1–6]

The silica matrices are particularly attractive because of their intrinsic chemical stability and biocompatibility. Silica is an essential component of cells in the human body and amorphous silica is known to be non-toxic and biodegradable.[9] Amorphous silica is ultimately excreted *via* the urine. Further, when the surface is functionalised, mesoporous silica can be readily internalised by plant and animal cells and is reported to have shown no significant cytotoxicity.[7]

A particularly significant advancement in the field has been the ability to engineer controlled porosity in these materials for applications such as drug delivery. The silica particle acts as a shield for its cargo molecule (*i.e.* drugs or peptides or proteins) and is expected to transport its cargo to the desired site without any significant loss prior to localisation. The release of the cargo molecules can then be triggered by change in pH at the target site or degradation of the particle *in vivo*. Control of such processes is only possible if the silica materials can be produced with well-defined surface areas and tuneable pores sizes and volumes.

The release mechanism of biodegradable polymer-based drug delivery systems relies on hydrolysis of the carrier, often triggered by suspension in water. For these materials the cargo must be loaded using organic solvents. Organic solvents are not always ideal for biological product as they can trigger denaturation or aggregation of the proteins.

For many mesoporous silica nanoparticles, absorption to the surface of the pores is reported to be controlled by size or morphology of the pores.[10] However it is difficult to predict under

[a]*Centre for Antimatter-Matter Studies (CAMS) at the Australian Nuclear Science and Technology Organisation (ANSTO), Menai, NSW, 2234, Australia. E-mail: suzanne.smith@ansto.gov.au*
[b]*Centre for Antimatter-Matter Studies (CAMS) at the Australian National University, Canberra, ACT, 0200, Australia*
[c]*Exilica Ltd, The Technocentre, Puma way, Coventry, CV1 2TT, UK*
[d]*Institute of Applied Physics, University of Tsukuba, Tsukuba, Japan*

what conditions the cargo molecules can be loaded and released. Therefore formulation for uptake and release must be determined for each cargo molecule and application. This is largely because it is difficult to determine the actual charge within the pores of the material. Some researchers have reported that the pore size does not influence the release of the cargo.[11] Other researchers have reported that the morphology of mesoporous silica nanomaterials controls the release behaviour.[12] This tends to suggest that the pores are of one type and therefore the affinity between the pore surface and the cargo molecule governs the release rate and not the size of the pores.

Understanding how the synthetic process changes the overall size and porosity of the particle is crucial for optimising the design of such systems. Numerous tools are used to provide information on the porosity in these types of materials, they include Small Angle Neutron Scattering and X-ray spectroscopy (SANS, SAXS), nitrogen gas adsorption-desorption, Brunauer Emmett Teller (BET), Scanning Electron Microscopy (SEM), Transmission Electron Microscopy (TEM) and Positron Annihilation Lifetime Spectroscopy (PALS).[13] Collectively they can provide information about the surface area and potentially the size and concentration of pores in the material. Positron annihilation technique is the powerful characterization tool for studying the size and concentration of free volume and defects in materials. The material is exposed to a ^{22}Na source and the lifetime of the positron in the material is used to determine the micropore size. The positron lifetime (τ) is the reciprocal of the integral of the positron $\rho_+(r)$ and the electron $\rho_-(r)$ densities at the site where the annihilation takes place.

$$\tau = \text{constant } x \left(\int \rho_+(r)\, \rho_-(r)\, \mathrm{d}r\right)^{-1} \quad (1)$$

A PAL spectrum of a polymer is usually found to consist of three different types of mean lifetimes (free positron, *para*-positronium and *ortho*-positronium) which correspond to different annihilation processes. For example, eqn (1) shows that a larger pore, which has a lower average electron density, is expected to have a longer positronium lifetime and is generally attributed to *ortho*-positronium formation.

However, these tools provide little information about the chemistry within the nanopores of the silica shells for loading the desired cargo molecules. Hence the pharmaceutical industry has to investigate a wide range of conditions (through trial and error) in order to determine the best condition for loading and release of molecules. The study of absorption of cargo agents (metals and/or drugs) to solid materials is generally performed using techniques such as atomic absorption spectroscopy, X-ray fluorescence spectroscopy, inductive coupled plasma-atomic emission spectrometry (ICP-AES), chelate titration, polarographic analysis, X-ray photoelectron spectroscopy, ATR/IR spectroscopy, electron spin resonance (ESR) spectroscopy and UV/Vis spectroscopy. Such techniques require either large test samples or solutions, or have comparatively complex testing procedures to determine the amount of cargo molecule absorbed. These methods can be extremely costly in time and use of expensive cargo molecules (*i.e.* drugs, peptides and proteins).

An alternative approach is the use of radiotracers, either the radioisotope of the metal ion of interest or a radioisotopic analogue to quantitatively track the movement of common cargo molecules within and from the materials. Gamma emitting radioisotopes are particularly useful as the gamma signal can be easily detected in various phases (i.e solid and liquid) using a gamma counter and they are highly sensitive. Test samples can be kept to a minimum (milligrams and microlitres) and analysis is rapid (secs) without a significant amount of processing. Furthermore, studies can be conducted under a range of solvent conditions including high electrolyte concentrations.[14,15,16]

This study reports the development and application of a library of radiotracers (nuclear sensors) of varying size, charge and hydrophobicity. Radiometal complexes of a series of ligands (see Fig. 1) were prepared to probe the chemistry and the availability of the pores within a hollow silica shell material.[17] The effect of pH on the binding and release from the hollow silica particles is presented. The intent of this work is to develop a library of nuclear

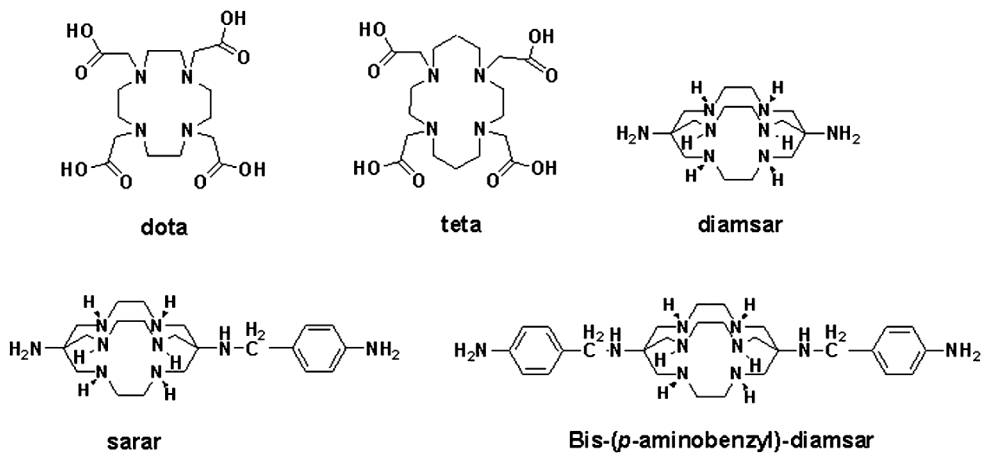

Fig. 1 Selected ligands radiolabelled for investigating binding properties of hollow silica shells. Ligand abbreviations: 1,4,7,10-tetraazacyclododecane-1,4,7,10-tetraacetic acid (dota); 1,4,8,11-tetraazacyclo-dodecane-1,4,8,11-tetraacetic acid (teta); 3,6,10,13,16,19-hexaazabicyclo[6.6.6]eicosane-1,8-diamine (diamsar); 1-*N*-(4-aminobenzyl)-3,6,10,13,16,19-hexaazabicyclo[6.6.6]eicosane-1,8-diamine (sarar); bis-(1-*N*-(4-aminobenzyl)-3,6,10,13,16,19-hexaazabicyclo[6.6.6]eicosane-1,8-diamine (bis-(*p*-aminobenzyl)-diamsar). Metal complexes of these ligands will be denoted as $(\text{M-ligand})^{n+}$, *e.g.* $(\text{Co-diamsar})^{2+}$.

Table 1 Retention factor (R_f) and mobile phases used to separate the $^{57/nat}Co^{2+}$ and each $^{57/nat}$Co-Ligand system

Mobile phase	$^{57/nat}Co^{2+}$ R_f	$^{57/nat}$Co-Ligand R_f
0.1 M sodium acetate pH 4.5: H_2O: MeOH: ammonium hydroxide 20 : 18 : 2 : 1 v/v); used to separate $(^{57/nat}Co\text{-dota})^{2-}$ from free $^{57/nat}Co^{2+}$	<0.2	>0.8
0.15 M ammonium acetate pH 6.5; used to separate $(^{57/nat}Co\text{-diamsar})^{2+}$, $(^{57/nat}Co\text{-sarar})^{2+}$ or $(^{57/nat}Co\text{-bis-}(p\text{-aminobenzyl})\text{-diamsar})^{2+}$ from free $^{57/nat}Co^{2+}$	>0.8	<0.2

sensor to determine the chemistry within porous materials in order to optimize their design and application as delivery vehicles.

Experimental

Materials and equipments

All reagents and solvents used were of analytical grade and obtained from commercial sources. Hollow silica shells were supplied by Exilica Ltd, The Technocentre, Puma Way, Coventry, CV1 2TT, UK. Water used for experimental purposes was Milli-Q grade (18 Ω cm). Buffers and mobile phases in this study were prepared as required.

High specific activity (SA) radioisotopes $^{57}Co^{2+}$ ($t_{1/2}$ = 271.8 days; SA = 2.59 × 10^5 GBq g^{-1}) and $^{64}Cu^{2+}$ ($t_{1/2}$ = 12.7 h; SA = 1.28 × 10^6 GBq g^{-1}) were obtained from MDS Nordion and ANSTO Radiopharmaceuticals and Industrials (ARI) respectively. The gamma emissions used to monitor each radioisotope were 122.1 and 136.5 keV for $^{57}Co^{2+}$ and 511 keV for $^{64}Cu^{2+}$. Analytical standard solutions of $CoCl_2$ (0.01 M) and $CuCl_2$ (0.01 M) were supplied by Sigma Aldrich and Riedel de Haen respectively. $CuCl_2$, $CoCl_2$ and 1,4,7,10-tetraazacyclododecane-1,4,7,10-tetraacetic acid (dota), 1,4,8,11-tetraazacyclododecane-1,4,8,11-tetraacetic acid (teta) were purchased from Sigma Aldrich and Macrocyclics (USA) respectively.

The equipment used for the binding and loading capacity studies include Eppendorf 5804R centrifuge, Wallac Wizard 1480 gamma counter and MyLab SLRM-2 M Intelli Mixer rotomix. Mass spectroscopy was conducted using AB Applied Biosystems MDS SCIEX API 2000 LC/MS/MS System mass spectrometer with an electrospray positive ionization method. Bruker Avance DPX 400-^{1}H NMR (400 MHz), ^{1}H recorded in D_2O; chemical shifts for ^{1}H signals for each compound were measured relative to the internal standard of dioxane. ^{1}H NMR (D_2O) δ: 3.75 (s).

Preparation of hollow silica shells

The procedure for fabricating silica shells used is summarised below and detailed elsewhere.[17] Poly(1-methylpyrrol-2-ylsquaraine) (PMPS) were prepared by refluxing equimolar amounts of 1-methylpyrrole and squaric acid in butan-1-ol for 18 h. The particles formed were filtered and washed (using a Soxhlet) with hot ethyl acetate. To the PMPS beads (1 g) was added 30 mL of 9 : 1 TEOS:ethanol and the mixture was sonicated for 10 s and magnetically stirred for a further 30 min. The resultant product was vacuum filtered and then suspended in 0.1 M HCl and stirred for 30 min. The PMPS beads were filtered off and then transferred to a crucible. The crucible was heated from 150 °C to 660 °C at 10 °C min^{-1}. The temperature was then held at 660 °C such that the overall time in the furnace was 3 h. After such time the sample was removed to cool at ambient temperature.

Table 2 Lifetime components for hollow silica shells and Co-doped hollow silica shells

Sample	τ_2(ns)	τ_3(ns)	τ_4(ns)	R_2(nm)	R_3(nm)	R_4(nm)
No.1	1.017 ± 0.03	2.57 ± 0.05	17.8 ± 0.2	0.34	0.67	1.68
No.2	0.64 ± 0.01	2.33 ± 0.02	—	0.18	0.62	—

Co-doped hollow silica shells

To 300 mg of hollow silica shells was added 0.1 M potassium dihydrogen phosphate (PBS) solution (5 mL), vortexed and the beads left to swell for 5 min. To the suspension was added cobalt(II) chloride (0.82 g) in PBS. The mixture was then left to agitate for 24 h and then centrifuged (1000 rpm for 1 min) and the supernatant decanted off. The Co-doped hollow silica shells were washed with Milli-Q water (3 × 1 mL), dried in air and analysed by PALS.

PALS (Positron Annihilation Life-time Spectroscopy) analysis

The lifetime spectra of the positrons were measured by using a digital oscilloscope (LeCroy Wavepro) and two scintillation detectors based on Hamamatsu H3378 photomultiplier tubes and BaF_2 scintillators.[18] About 4 × 10^6 counts were accumulated for each lifetime spectrum. The lifetime spectrum of positrons, $S_{LT}(t)$, is given by

$$S_{LT}(t) = \sum \lambda_i I_i \exp(-\lambda_i t), \quad (2)$$

where λ_i and I_i are respectively the i-th components of the annihilation rate of positrons and its intensity.

The lifetime of the positrons, τ_i, is given by $1/\lambda_i$. The observed spectra were analysed with a time resolution of about 170 ps (full-width-at-half-maximum, FWHM) by using the RESOLUTION computer program.[19] The data are presented in Fig. 2, 3 and Table 2.

Synthesis of hexa-aza cages

(Cu-diamsar)$^{2+}$. Diamsar was prepared in a similar manner to that previously described and characterised by ^{1}H NMR.[20] The $CuCl_2$ (1.28 g; 11.5 mmol) was added to diamsar in ethanol (3.0 g; 9.55 mmol; 100 mL). The blue solution formed was evaporated to dryness under reduced pressure and the residue (Cu-diamsar)Cl_2 (4.8 g) used without further purification for the synthesis of (Cu-(*p*-nitrobenzyl)-diamsar)$^{2+}$ and (Cu-bis-(*p*-nitrobenzyl)-diamsar)$^{2+}$.

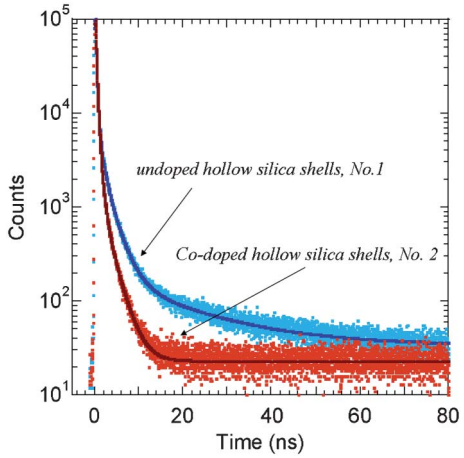

Fig. 2 Positron Annihilation Life-time Spectroscopy (PALS) spectrum of hollow silica shells.

(Cu-(*p*-nitrobenzyl)-diamsar)$^{2+}$ and (Cu-bis-(*p*-nitrobenzyl)-diamsar)$^{2+}$

The complexes were prepared using a modified literature procedure.[21] The (Cu-diamsar)Cl_2 (2.5 g; 5.58 mmol) was dissolved in ethanol water solution (w/w 1 : 1; 50 mL). The pH of the solution was adjusted to 4.5 by the addition of 4% NaOH solution. Then the 4-nitrobenzaldehyde (1.18 g; 7.81 mmol) and sodium cyanoborohydride (0.42 g; 6.68 mmol) were added and the reaction mixture was left to stir under nitrogen gas for 5 h at 23 °C. The ethanol was then evaporated off and the blue solution diluted in water (2 L) and loaded onto a Sephadex SP C-25 column (55 × 7.5 cm swelled in water). The column was washed with various sodium citrate solutions (1 L of 0.1 M followed by 4 L of 0.3 M). Three fractions representing three blue bands on the column were collected. They represent (Cu-diamsar)$^{2+}$, (Cu-(*p*-nitrobenzyl)-diamsar)$^{2+}$ and (Cu-bis-(*p*-nitrobenzyl)-diamsar)$^{2+}$ in order of elution. Each fraction was diluted in water (3 fold) and then absorbed on to three different Dowex 50 W × 2 columns (10 × 1.2 cm swelled in water) and washed with water at a flow rate of 14 mL min^{-1}. The respective columns were then washed with 1 M HCl (1 L) and respective copper complexes were eluted with 6 M HCl. Each fraction was evaporated to dryness under vacuum and the resultant residue dissolved in water (2 × 40 mL) and rotary evaporated to dryness. The addition of absolute ethanol (20 mL) to the residue and sonication for 3 min resulted in the precipitation of blue crystals. The crystalline product was filtered and washed with 10 mL of cold ethanol and dried under vacuum. Yield for (Cu-(*p*-nitrobenzyl)-diamsar)$^{2+}$ and (Cu-bis-(*p*-nitrobenzyl)-diamsar)$^{2+}$ were 0.81 g (29%) and 0.38 g (11%) respectively. An electrospray mass spectrometry (ESI/MS) in an aqueous solution (10^{-6} M) at a cone voltage of 25 V was conducted. (Cu-(*p*-nitrobenzyl)-diamsar)$^{2+}$; ESI/MS: displayed a major signal at m/z = 547.2 [M+ HCl]$^+$ and m/z = 256.2 [M+ 2H]$^{2+}$ with a minor signal of m/z 511.4 [M + H]$^+$. (Cu-bis-(*p*-nitrobenzyl)-diamsar)$^{2+}$; ESI/MS: displayed a major signal at m/z = 682.4 [M+ HCl]$^+$ and m/z = 324.0 [M+ 2H]$^{2+}$ with a minor signal of m/z 646.5 [M + H]$^+$.

(bis-(*p*-aminobenzyl)-diamsar)$^{2+}$

Sodium borohydride (600 mg; 1.59 mmol) in water (0.5 mL) was slowly loaded on to the catalyst [10% palladium on activated charcoal] (110 mg) under nitrogen. The (Cu-(bis-*p*-nitrobenzyl)-diamsar)$^{2+}$ (384 mg; 0.06 mmol) dissolved in NaOH solution (0.5 mL; 0.04% NaOH) was then added slowly to the suspension under nitrogen. The reaction was allowed to proceed until the colour of the solution turned from blue to clear (30 min at 23 °C). The Pd/C catalyst was filtered off (0.22 μm) and hydrochloric acid (1 M) was added dropwise until gas evolution ceased (~0.5 mL, 1 M HCl). The clear solution was lyophilised to produce a white powder. ^{1}H NMR: 3.00 (s, 12H, NCH_2CH_2N); 3.31 (s, 12H, NCCH_2N); 3.96 (s, 4H, ArCH_2); 6.94 (d, 4H, Ar–*H*); 7.34 (d, 4H, Ar–*H*); ESI/MS, m/z = 525.6 [M + H]$^+$.

Sarar

Sarar was synthesized using a similar procedure as previously described.[21]

Sodium borohydride (380 mg; 10.0 mmol) in water (0.6 mL) was slowly loaded on to the catalyst [10% palladium on activated charcoal] (65 mg) under nitrogen. The

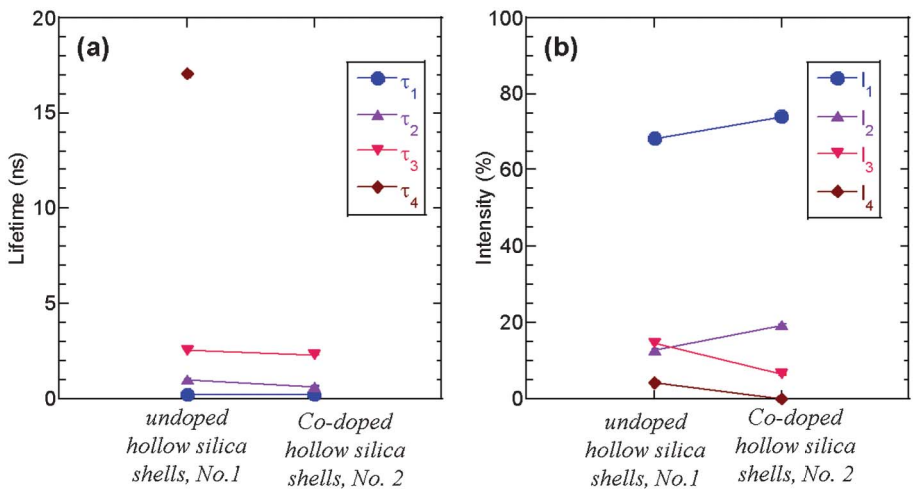

Fig. 3 The lifetime and relative intensities of micropores in undoped and Co-doped hollow silica shells.

(Cu-(*p*-nitrobenzyl)-diamsar)$^{2+}$ (500 mg; 0.76 mmol) dissolved in NaOH solution (0.4 mL; 0.04% NaOH) was then added slowly to the suspension under nitrogen. The reaction was allowed to proceed until the colour of the solution turned from blue to clear (20 min at 23 °C). The Pd/C catalyst was filtered off (0.22 μm) and hydrochloric acid (1 M) was added dropwise until gas evolution ceased (~0.7 mL, 1 M HCl). The clear solution was lyophilised to produce a white powder. ^{1}H NMR: 2.92 (s, 12H, NCH_2CH_2N); 3.00 (s, 6H, NCCH_2N); 3.10 (s, 6H, NCCH_2NCCH_2); 3.58 (s, 2H, ArCH_2); 6.81 (d, 2H, Ar–*H*); 7.13 (d, 2H, Ar–*H*); ESI/MS, m/z = 420.4 [M + H]$^+$.

Complexation of $^{57/nat}Co^{2+}$ by dota, diamsar, sarar and bis-(*p*-aminobenzyl)-diamsar - ($^{57/nat}$Co-Ligand)

A typical procedure involved exposing equimolar amounts (1.5×10^{-2} M) of the Ligand (dota, diamsar, sarar or bis-(*p*-aminobenzyl)-diamsar) to a Co^{2+} solution doped with $^{57}Co^{2+}$ in sodium phosphate buffer (PBS) pH 7. The mixture was then vortexed for 5 s and incubated at 23 °C for 1 h. The total volume of the final solutions was 480 μL. The complexation reaction was monitored at 23 °C by instant thin layer chromatography (ITLC-SG) until > 95% of the $^{57/nat}$Co-Ligand was formed. The mobile phase and retention factor (R_f) for $^{57/nat}Co^{2+}$ and $^{57/nat}$Co-Ligand are summarised in Table 1. The percentage of $^{57/nat}Co^{2+}$ complexed by the Ligand was calculated for each reaction.

Uptake of $^{64/nat}Cu^{2+}$, $^{57/nat}Co^{2+}$, ($^{57/nat}$Co-dota)$^{2-}$, ($^{57/nat}$Co-diamsar)$^{2+}$, ($^{57/nat}$Co-sarar)$^{2+}$ and ($^{57/nat}$Co-bis-(*p*-aminobenzyl)-diamsar)$^{2+}$ by hollow silica shells

A typical procedure involved mixing 10 mg (accurately weighed in triplicate) of hollow silica shells in 1480 μL of appropriate buffer (pH 3–9) at 23 °C. Buffer solution ranged from 0.1 M glycine in 0.1 M sodium chloride for pH 3.0; 0.1 M sodium acetate for pH 4.0 and 5.0; 0.1 M potassium dihydrogen phosphate for pH 6.0, 7.0 and 8.0; 0.1 M glycine in 0.1 M sodium chloride, pH adjusted with sodium hydroxide to pH 9.0. The resulting mixture was then vortexed for 5 s and left to agitate for 5 min. The hollow silica shells were then exposed to either free $^{57/nat}Co^{2+}$ or $^{64/nat}Cu^{2+}$ (1×10^{-3}M) or $^{57/nat}$Co-Ligand (1×10^{-4}M) in 20 μL. Uptake of the metal ions and $^{57/nat}$Co-Ligand were monitored until equilibrium was reached. At set time intervals (0, 5, 10, 30, 60, 90, 120 min and 24 h) the reaction mixture was centrifuged (7.5 rpm for 2 min). The supernatant was sampled (20 μL in triplicate) and the radioactivity associated with solutions and hollow silica shells were measured using the gamma counter. The moles of metal (**M**) ions and metal–ligand complex (**M-Ligand**) associated with the hollow silica shells were calculated for each time point using eqn (3). In addition, the distribution coefficients (K_d) at the various time intervals were calculated as outlined in eqn (4).

$$A = \frac{B \times \%\ \text{activity associated with hollow silica shells}}{\text{weight (mg) of hollow silica shells}} \quad (3)$$

Where A = moles of **M** ion or **M-Ligand** bound to milligrams of hollow silica shells and B = initial moles of **M** ion or **M-Ligand**

$$K_d = \frac{(\%C/m)}{(\%D/V)} \quad (4)$$

Where C = **M** ion or **M-ligand** bound to hollow silica shells
D = **M** ion or **M-ligand** in solution
m = amount of hollow silica shells (mg)
V = total volume of the solution (mL)

Release of $^{64/nat}Cu^{2+}$, $^{57/nat}Co^{2+}$, and $^{57/nat}$ Co-Ligand from hollow silica shells

The hollow silica shells were loaded with each nuclear sensor [*i.e.* $^{64/nat}Cu^{2+}$, $^{57/nat}Co^{2+}$, ($^{57/nat}$Co-dota)$^{2-}$, ($^{57/nat}$Co-diamsar)$^{2+}$, ($^{57/nat}$Co-sarar)$^{2+}$ or ($^{57/nat}$Co-bis-(*p*-aminobenzyl)-diamsar)$^{2+}$ in a similar manner to that described above and once equilibrium was reached, centrifuged (7.5 rpm for 2 min) and the supernatant removed carefully. The loaded hollow silica shells were then exposed to a fresh solution of buffer (1.5 mL) and vortexed for 5 s. The mixtures were left to agitate at 23 °C up to 24 h. Then solutions were sampled for the release of nuclear sensor over varying time intervals (10, 30, 60, 90, 120 min and 24 h) in a similar to that described above. The radioactivity associated with solutions and hollow silica shells were measured in a gamma counter. As described above the moles of **M** ion and **M-Ligand** associated with the hollow silica shells were calculated at each time point.

Results and discussion

Preparation of hollow silica shells and measurement of porosity

The hollow silica shells were prepared by the over-coating of sacrificial polymeric template particles with a silicon precursor followed by thermal calcination in a furnace at 660 °C. The hollow silica shells were specifically designed to act as molecular containers. They have a thin permeable shell to promote increased flow of target molecules and solution into and from the shells. The surface area (SSA) of the hollow silica shells was determined using the BET isotherm to be > 370 m^2 g^{-1}.[22]

In the present study, positron annihilation lifetime spectroscopy (PALS) was used to determine the microporosity in the hollow silica shells. The probability or intensity of *ortho*-positronium formation is proportional to the number of free pores in hollow silica shells. A comparison of spectra for undoped and Co-doped hollow silica shells is illustrated in Fig. 2. Visual analysis of the spectra shows there is a sharp decrease in the intensity of the Co-doped silica shell spectrum compared to that of the metal free sample. This clearly reflects a change in the sample. Fig. 3 and Table 2 summarises the analysis of these spectra and the determined life-time and intensity of the free positrons and positronium formation (pick-off annihilations) on exposure to the ^{22}Na source.

Analysis of the results using eqn (1) show the spectrum (No.1) for the hollow silica shells decomposed into four components [τ_i where i = 1 to 4] (see Fig. 3a). The pore diameters within the hollow silica shells were estimated from the lifetimes of each *ortho*-positronium component using the Tao–Eldrup model.[23] From Fig. 3(a) we can see that the hollow silica shells have four lifetime components (τ_1 to τ_4) while Co-doped silica shells have only three lifetime components (τ_1 to τ_3). The second and third lifetimes present in both spectra appear to be due to pick-off annihilation of Ps and relate to two pore sizes of 0.34 nm and 0.67 nm radii. The longest lifetime, τ_4 found present only in the hollow silica

shell relates to the presence of a larger pore of 1.68 nm radius. Fig. 3(b) show the relative intensity of each τ value. It show the disappearance of the τ_4 lifetime (intensity 0%) in the Co-doped samples. This suggests that the major trapping of the Co(II) ion occurs in the larger pore of 1.68 nm.

Preparation of hexa aza cage derivatives

The hexa aza cage systems were synthesised *via* a metal template synthesis of the Co(II)-diamsar species as previously described.[20] The cobalt ion was removed using sodium cyanide followed by extraction into acetonitrile. The recrystallised diamsar is then complexed with a slight excess of copper chloride and reductive amination of $(Cu\text{-diamsar})^{2+}$ with *p*-nitrobenzaldehyde afforded both the copper complex of the bis and mono alkylated species of diamsar $(Cu\text{-}(p\text{-nitrobenzyl})\text{-diamsar})^{2+}$ and $(Cu\text{-bis-}(p\text{-nitrobenzyl})\text{-diamsar})^{2+}$ respectively, as the hydrochloride salt. The final products were purified on a Sephadex SP C-25 and Dowex 50 W × 2 columns. The mass spectra analysis gave for $(Cu\text{-}(p\text{-nitrobenzyl})\text{-diamsar})^{2+}$ a major signal at $m/z = 547.2$ $[M+ HCl]^+$ and $m/z = 256.2$ $[M+ 2H]^{2+}$ with a minor signal of m/z 511.4 $[M + H]^+$. and $(Cu\text{-bis-}(p\text{-nitrobenzyl})\text{-diamsar})^{2+}$ a major signal at $m/z = 682.4$ $[M+ HCl]^+$ and $m/z = 324.0$ $[M+ 2H]^{2+}$ with a minor signal of m/z 646.5 $[M + H]^+$, indicating pure products (in supplementary material). The de-metallation from the cage was performed by using the reducing agent sodium borohydride with palladium on carbon in basic media. This afforded sarar and bis-(*p*-aminobenzyl)-diamsar (Fig. 1) as a white powder. All other Ligands were obtained from commercial sources.

Preparation of nuclear sensors

A range of nuclear sensors (radiotracers) was prepared for investigating the chemical properties of porous materials. All ligands (see Fig. 1) were chosen based on their ability to form thermodynamically stable complexes with Cu^{2+} or Co^{2+} metal ion.[24,25]

Stability constants (log *K*) reported for dota complexes of Hg^{2+}, Cu^{2+}, Ni^{2+} and Co^{2+} are 26.4, 22.2, 20.0 and 20.2 at 25 °C, [0.1 M $(CH_3)_4N(NO_3)$] respectively and 25.7, 21.6, 19.9 and 16.6 respectively for teta.[26–28] The Hg^{2+} complex with sar, the parent hexa aza cage of sarar, log *K* is 28.1 ($[OH^-] = 0.1$ M, $I = 0.5$ M $NaClO_4$, at 25 °C), which is significantly larger than the Hg^{2+} dota or teta complexes.[29] The $[Cu(sar)]^{2+}$ complex is expected to be even more stable but the very slow dissociation of the Cu^{2+} cation precludes the determination of its log *K* value. The exchange of radiolabelled Cu^{2+} ion with the copper complex (< 6% in 18 h at ~ 25 °C) is consistent with this analysis.

Each ligand was radiolabelled with either $^{nat/57}Co^{2+}$ or $^{nat/64}Cu^{2+}$ respectively.

The radiolabelling of each ligand was performed by mixing the metal ion (**M**) with the Ligand (**L**) at a molar ratio of 1 : 1 at ~10^{-2} M and room temperature. ITLC was used to monitor the complexation of the **M** ion. Once the complexation reaction was complete the final products were diluted in the various buffer solutions and monitored for breakdown over time. Those complexes that demonstrated stability over a 24 h period were used for the binding studies. Fig. 4 shows the percentage of **M** ion complexed by selected ligands at millimolar concentrations after 1 h at pH 7.

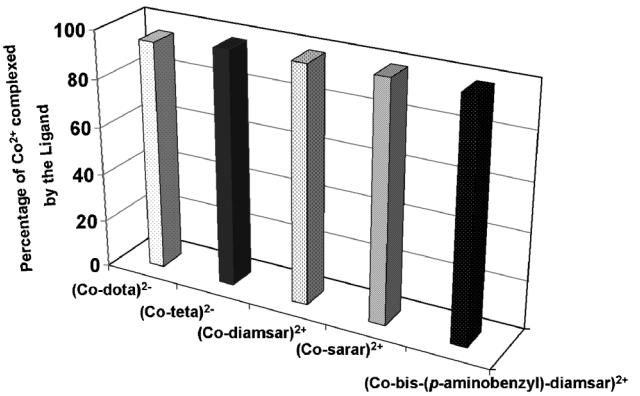

Fig. 4 Percent of $^{57/nat}Co^{2+}$ complexed by dota, teta, diamsar, sarar and bis-(*p*-aminobenzyl)-diamsar after 1 h. $[M^{2+}] = 10^{-3}$ mol L^{-1}; Buffer: 0.1 mol L^{-1} PBS pH 7; $T = 23$ °C; Time = 1 h.

Metal (M) binding properties of hollow silica shells

An accurately weighed amount of hollow silica shells was incubated in buffer solutions (*i.e.* pH 3–9) at room temperature for at least 5 min. The suspensions were then exposed to each nuclear sensor and the resultant reaction mixture was then sampled at varying time intervals (5 min to 24 h) after centrifugation. The amount of nuclear sensor bound to the hollow silica shells was determined by counting in a gamma counter. Fig. 5 to 8 illustrate selected data.

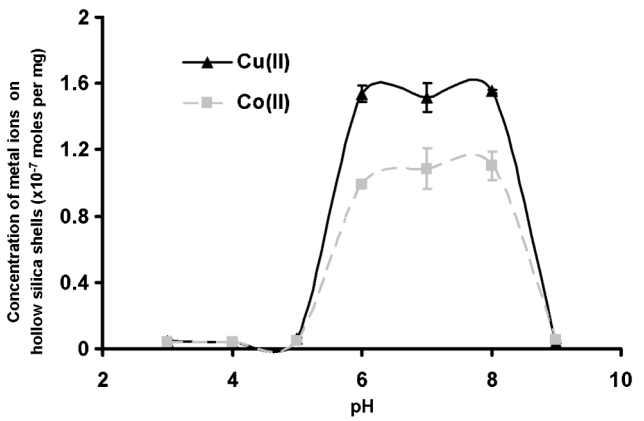

Fig. 5 The effect of pH on metal binding properties of hollow silica shells at ambient temperature. $[M^{2+}] = 10^{-3}$ mol L^{-1}; silica shell = 10 mg; V = 1.5 mL; Time = 10 min; $T = 23$ °C; number of samples (n) = 3.

Fig. 5 illustrates the binding profile for Cu^{2+} and Co^{2+} over a range of pH. The data clearly indicate the absorption of these metal ions is dependent on pH, with maximum absorption occurring over pH 6–8. While the absorption curves for Cu^{2+} and Co^{2+} are similar, the total amount of **M** ion bound and the rate at which equilibrium is reached were significantly different for the two metal ions. The total amount of Cu^{2+} bound was 1.5 fold higher than Co^{2+} in pH 8 buffer. The rate at which the Cu^{2+} ion was absorbed was

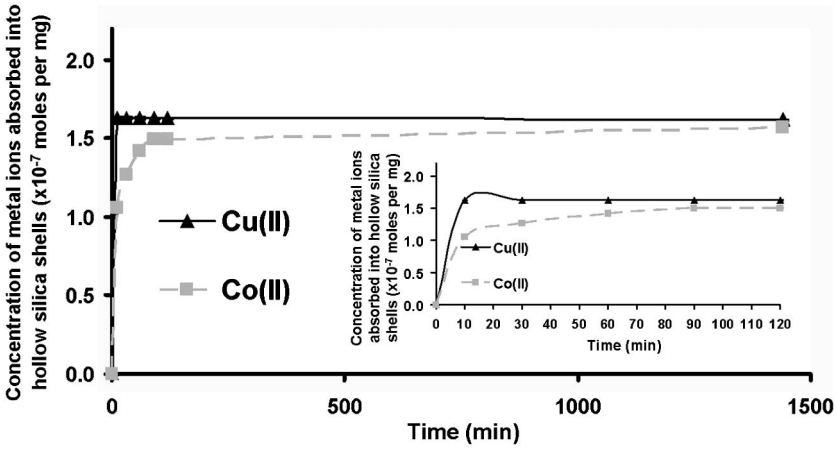

Fig. 6 Metal ion bound to hollow silica shells verses time at pH 8. $[M^{2+}] = 10^{-3}$ mol L^{-1}; silica shell = 10 mg; $V = 1.5$ mL; $T = 23$ °C; number of samples (n) = 3.

considerably faster than Co^{2+} ion, reaching maximum absorption within 10 min compared to 90 min for the latter species (see Fig. 6).

Low uptake of both metal ions at pH 3 to 5 indicates the pores of the hollow silica shells are most likely negatively charged, attracting the H^+ ion more readily. In contrast, the poor uptake at pH 9 is mostly likely due to either the Cu^{2+} and Co^{2+} ion preferentially binding to buffer (*i.e.* glycine) or the formation of soluble hydroxide species. ITLC was used to monitor the formation of metal hydroxide species (R_f 0) in the absence of hollow silica shells and was found to be absent. Only at a Co^{2+} concentration of 0.75 x10^{-2} M in glycine buffer (pH 9) is there any evidence of precipitation, hence it is more likely for the present studies the Co^{2+} is forming complexes with glycine buffer. Thus the Co^{2+} complex is not as readily available for the uptake by hollow silica shells. Overall the metal ion binding properties of the hollow silica shells at pH 6–8 correlates well with the desolvation energies for inner sphere H_2O from the respective metal ion (*i.e.* $Cu^{2+} = \sim 5 \times 10^8$ s^{-1} and $Co^{2+} = \sim 4 \times 10^5$ s^{-1}).[30] The affinity and total amount of metal ion bound correlates with the Irving William series $Cu^{2+} > Co^{2+}$.

Metal complex (M-Ligand) binding properties of hollow silica shells

The uptake of each **Co-Ligand** species by the hollow silica shells was also monitored over time (up to 24 h) or until equilibrium was reached at each pH. The moles of nuclear sensor associated with the hollow silica shells (10 mg) were calculated at each time point. In general, the **M-Ligand** absorption by the hollow silica shells was selective and rapid at room temperature. The reactions were often complete within 10 min with mild shaking or 1 min with vortexing. Fig. 7 and 8 illustrate selected results.

Fig. 7 compares the binding of a series of nuclear sensors to the hollow silica shells over a range of pH. The data show how the effect of charge and hydrophobicity of **M-Ligand** can significantly influence its binding to the hollow silica shells. The positively charged nuclear sensors; $(Co\text{-diamsar})^{2+}$, $(Co\text{-sarar})^{2+}$ and (Co-bis-(*p*-aminobenzyl)-diamsar)$^{2+}$ show increased binding affinity as the pH is increased (from pH 5–9). Notably, negatively charged species $(Co\text{-dota})^{2-}$ were preferentially weakly absorbed at pH 3 and 4 compared to positively charged nuclear sensors. The binding affinity of the $(Co\text{-teta})^{2-}$ was also tested at pH 3 to 9 and found to behave in a similar manner to the $(Co\text{-dota})^{2-}$ over the same pH.

Of particular significance is the dramatic enhancement in the binding of the (Co-bis-(*p*-aminobenzyl)-diamsar)$^{2+}$ species at pH 6, 7 and 8 compared to both $(Co\text{-diamsar})^{2+}$ and $(Co\text{-sarar})^{2+}$. The binding affinity for all three of the positively charged **M-Ligand** species is equivalent at pH 9. In view of this, the binding of the positively charged **M-Ligand** was fast and in the following sequence Co-(bis-(*p*-aminobenzyl)-diamsar)$^{2+}$ > $(Co\text{-diamsar})^{2+}$ > $(Co\text{-sarar})^{2+}$ at pH 9 (see Fig. 8). Comparison of the rate of uptake for these hexa aza cage complexes by hollow silica shells over time show that with the more hydrophobic species, [$(Co\text{-sarar})^{2+}$ and (Co-bis-(*p*-aminobenzyl)-diamsar)$^{2+}$], binding was complete in only 10 min, while equilibrium for $(Co(diamsar)^{2+}$ took 90 min. Data also show that the total amount absorbed for each nuclear sensor is equivalent at 1440 min.

Collectively it could be speculated that the pores within the hollow silica shells are most likely negatively charged and that affinity for the positively charged molecules will be preferred. In addition the more hydrophobic molecules will be absorbed preferentially at the high pH (neutral through to basic). This is consistent with the behaviour observed for the higher absorption of negatively charged species to the hollow silica shells at pH 3 to 4. At the lower pH the pores within the hollow silica shells are most likely protonated and the positively charged nuclear sensors can not compete for the binding sites as effectively as H^+ ion. The PALS study described earlier support the hypothesis that the nuclear sensors are most likely to be absorbed into the larger pore (radius = 1.68 nm) of the hollow silica shell.

Release of metal (M) and metal complexes (M-Ligand) from hollow silica shells

The binding studies were conducted over a range of pH in order to identify the conditions under which the nuclear sensor is stably bound and most likely to be released. Together with the PALS data they can assist to gain an understanding of whether the size or charge of the pores govern the binding properties, and ultimately how this information can be used to guide reengineering of these types of materials.

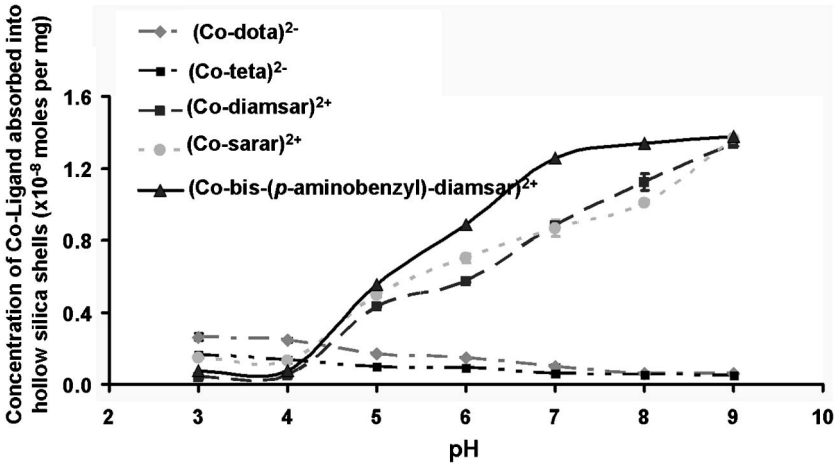

Fig. 7 Effect of pH on the binding of metal complexes (Co-Ligand) to hollow silica shells. [Co-Ligand] = 10^{-4} mol L^{-1}; silica shell = 10 mg; V = 1.5 mL; Time = 10 min; T = 23 °C; number of samples (n) = 3.

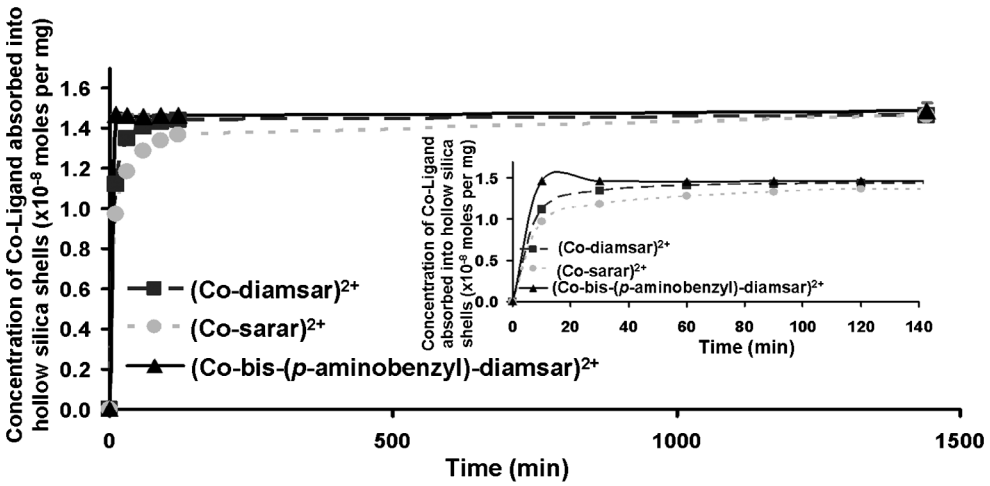

Fig. 8 Moles of $(Co\text{-}Ligand)^{2+}$ absorbed into hollow silica shells at pH 9 over time. $(Co\text{-}Ligand)^{2+}$ = 10^{-4} mol L^{-1}; silica shell = 10 mg; V = 1.5 mL; T = 23 °C; number of samples (n) = 3.

Depending on the results obtained in Fig. 7 hollow silica shells were loaded with the nuclear sensors at their optimum pH. The mixtures were centrifuged and the hollow silica shells loaded with the nuclear sensor were separated and re-exposed to fresh buffer solution of the same pH. Initial binding conditions for the **M** species, negatively and positively charged **M-Ligand** species were conducted at pH 6 to 8, pH 3 to 5 and pH 6 to 9, respectively. The mixtures were then vortexed and left to agitate at 23 °C for 24 h. The release of nuclear sensor was monitored over time. Fig. 9 to 11 show percentage of nuclear sensor released after 24 h.

Fig. 9 shows that twice as much Cu^{2+} ion (30.0 ± 0.4%) is released at pH 7 compared to Co^{2+} (16.0 ± 0.1%) after 24 h. For pH 6 and 8 the amount released for both metal ions is similar, (17.0 ± 0.4%). In contrast the negatively charged species $(Co\text{-}dota)^{2-}$ and $(Co\text{-}teta)^{2-}$ are released more rapidly, with ~50–60% and ~80% between pH 3–5, respectively after 24 h (see Fig. 10).

The positively charged hexaza cage complexes absorbed into hollow silica shells were exposed to solutions of pH 6 to 9 (see Fig. 11). Up to 20% [19.0 ± 0.2% to 20.0 ± 2.5%] $(Co\text{-}diamsar)^{2+}$ was released from hollow silica shells within minutes, with no

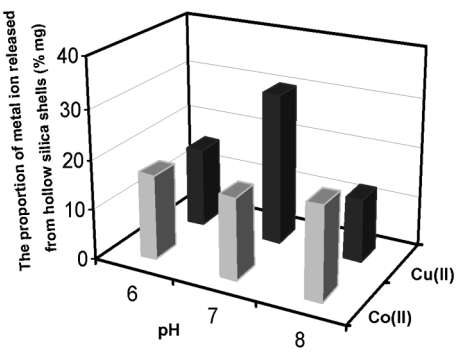

Fig. 9 Percentage of **M** released from hollow silica shells after re-exposure to fresh buffer solution. [M] = 10^{-6} mol L^{-1}; silica shell = 10 mg; V = 1.5 mL; T = 23 °C; number of samples (n) = 3.

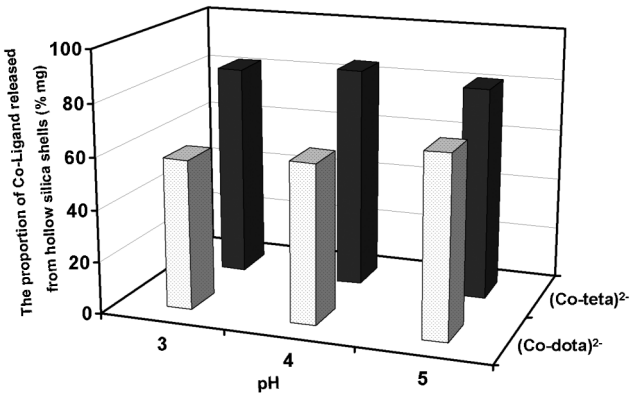

Fig. 10 Percent of $(Co\text{-}Ligand)^{2-}$ released from hollow silica shells after re-exposure to fresh buffer solution. [Co-Ligand] = 10^{-6} mol L^{-1}; silica shell = 10 mg; V = 1.5 mL; T = 23 °C; number of samples (n) = 3.

further loss over the study period of 24 h. For $(Co\text{-}sarar)^{2+}$ loss is highly dependent on pH with 50.0 ± 0.7%, 30.0 ± 0.7%, 10.0 ± 0.1% and 0% released after 24 h at pH 6, 7, 8 and 9, respectively. For the more hydrophobic nuclear sensor, (Co-bis-(*p*-aminobenzyl)-diamsar)$^{2+}$ the behaviour is quite different. There is 30.0 ± 0.7% and 35.0 ± 0.3% released at pH 7 and 9, respectively, and in contrast, less than 26.0 ± 0.2% is released at pH 6 and 8. As demonstrated with the Co-doped silica shells using PALS, the nuclear sensors are most likely absorbed into the larger pore (1.68 nm radius).

Distribution coefficients for nuclear sensors with hollow silica shells

Distribution coefficients (K_d) are often calculated in an effort to obtain an indication of strength of binding between a solute and resin in the presence of a specified solution. Distribution coefficients are generally used for metal purification where it is important to determine conditions of highest and weakest binding to the exchange resins. This information is then used to determine the optimum conditions for separation.

For the current study the K_d was determined by exposing a known quantity (10 mg) of hollow silica shells in a fixed volume (1.5 mL) and known concentration of nuclear sensors (1×10^{-4} M) and incubated with gentle agitation at 23 °C for 24 h in various buffer solutions. Selected data are given in Fig. 12 and 13. K_d values greater than 100 have been classified as moderate binders while those in the region of 1000 or more are considered to be high binding. Values in the region of 50 to 10 are weak binders and therefore would be released rapidly when exposed to the same buffer conditions. The data presented in this study (Fig. 13) show that the K_d value for $(Co\text{-}dota)^{2-}$ and $(Co\text{-}teta)^{2-}$ were lower than that for the positively charged **M-Ligand**. This may be attributed to the higher affinity of $(M\text{-}Ligand)^{2+}$ for exchange sites on the hollow silica shells. More importantly the high K_d indicates the optimum solvent conditions under which an agent should be bound and the large volumes of solvent that would be required to release the agent from the hollow silica shells.

Conclusion

The work presented here represents the first report of the application of radiometal complexes for the characterization of porous materials. The work clearly shows the absorption to the hollow silica shells is governed by size, charge and hydrophobicity of its micropores. The micropores in the hollow silica shells are sensitive to subtle changes in the molecular architecture of the ligands and their resultant complexes demonstrated by distinct changes in rate of absorption and release. The binding of the nuclear sensors is most likely due to hydrogen, electrostatic or ionic bonding. Distribution coefficients proved to be valuable and sensitive indicators of release rates, and potentially could be useful for defining formulation and application of the porous material.

The use of nuclear sensors was found to be a very sensitive and fast method for assessing the performance of porous materials. An advantage of this approach is the minimal amount of product required for analysis. The process is highly adaptable for high-throughput screening of the next generation of porous or controlled release materials. It has the potential to predict the type of molecules and the conditions under which they might be encapsulated by porous material. Using this strategy for the screening of porous materials may provide an opportunity for real cost savings in development of product formulations.

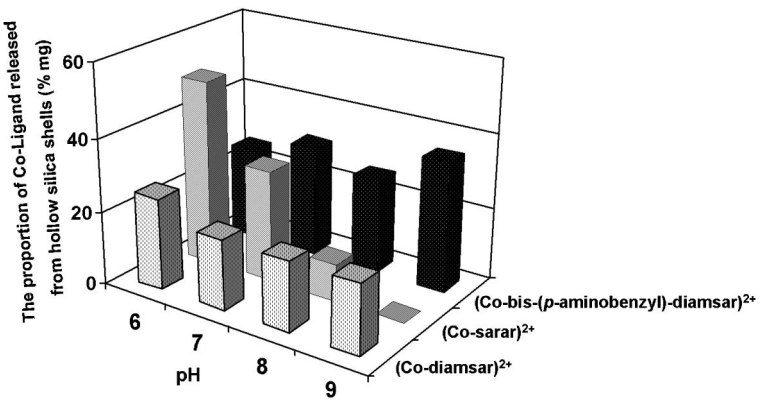

Fig. 11 Percent of $(Co\text{-}Ligand)^{2+}$ released from hollow silica shells after re-exposure to fresh buffer solution. [Co-Ligand] = 10^{-6} mol L^{-1}; silica shell = 10 mg; V = 1.5 mL; T = 23 °C; number of samples (n) = 3.

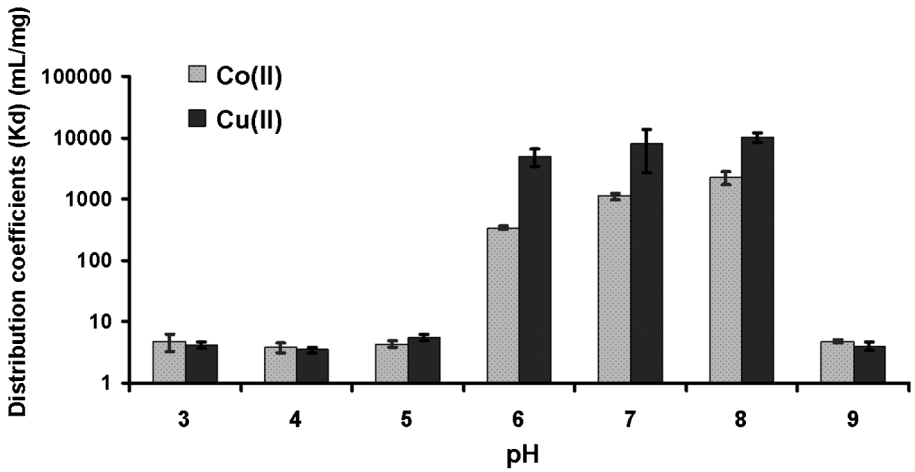

Fig. 12 Distribution coefficient of **M** after re-exposure to fresh buffer solution. [M] = 10^{-3} mol L^{-1}; silica shell = 10 mg; V = 1.5 mL; T = 23 °C; number of samples (n) = 9.

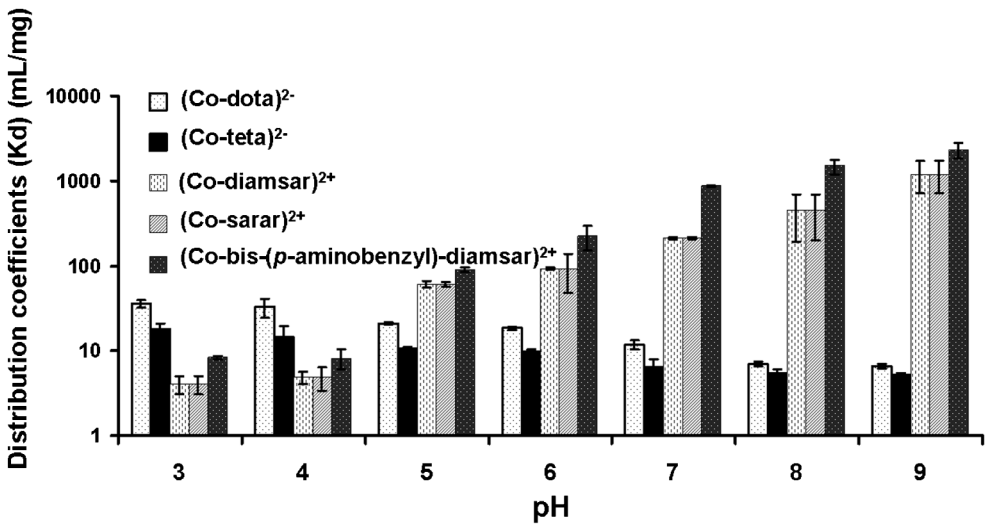

Fig. 13 Distribution coefficient of **M-Ligand** after re-exposure to fresh buffer solution. [M-Ligand] = 10^{-4} mol L^{-1}; silica shell = 10 mg; V = 1.5 mL; T = 23 °C; number of samples (n) = 9.

Acknowledgements

We thank Australian Research Council funding for the ARC Centre of Excellence for Antimatter-Matter Studies.

References

1 S. Huh, J. W. Wiench, J. C. Yoo, M. Pruski and V. S. Y. Lin, *Chem. Mater.*, 2003, **15**, 4247.
2 B. G. Trewyn, C. M. Whitman and V. S. Y. Lin, *Nano Lett.*, 2004, **4**, 2139.
3 K. Suzuki, K. Ikari and H. Imai, *J. Am. Chem. Soc.*, 2004, **126**, 462.
4 J. Y. Ying, *Chem. Eng. Sci.*, 2006, **61**, 1540.
5 J. Y. Ying, C. P. Mehnert and M. S. Wong, *Angew. Chem., Int. Ed.*, 1999, **38**, 56.
6 C. T. Kresge, M. E. Leonowicz, W. J. Roth, J. C. Vartuli and J. S. Beck, *Nature*, 1992, **359**, 710.
7 D. R. Radu, C. Y. Lai, K. Jeftinija, E. W. Rowe, S. Jeftinija and V. S. Y. Lin, *J. Am. Chem. Soc.*, 2004, **126**, 13 216.
8 I. Slowing, B. G. Trewyn and V. S. Y. Lin, *J. Am. Chem. Soc.*, 2006, **128**, 14792.
9 Chemwatch 10451 NC317TCP Version No: 3 CD 2010/4 Page 1 of 15.
10 M. Vallet-Regi, A. Rámila, R. P. del Real and J. Pérez-Pariente, *Chem. Mater.*, 2001, **13**, 308.
11 I. I. Slowing, B. G. Trewyn, S. Giri and V. S. Y. Lin, *Adv. Funct. Mater.*, 2007, **17**, 1225.
12 B. G. Trewyn, C. M. Whitman and V. S. Y. Lin, *Nano Lett.*, 2004, **4**, 2139.
13 S. V. Smith, *J. Phys.: Conf. Ser.*, 2009, **185**, 012044.
14 R. Naik, G. Wen, M. S. Dharmaprakash, S. Hureau, A. Uedono, X. Wang, X. Liu, P. G. Cookson and S. V. Smith, *J. Appl. Polym. Sci.*, 2010, **115**, 1642–1650.
15 R. Rajkhowa, R. Naik, L. Wang, S. V. Smith and X. Wang, *J. Appl. Polym. Sci.*, 2011, **119**, 3630–3639.
16 G. Wen, R. Naik, P. G. Cookson, S. V. Smith, X. Liu and X. G. Wang, *Powder Technol.*, 2010, **197**, 235.
17 D. E. Lynch, Y. Nawaz and T. Bostrom, *Langmuir*, 2005, **21**, 6572.
18 H. Saito, Y. Nagashima, T. Kurihara and T. Hyodo, *Nucl. Instrum. Methods Phys. Res., Sect. A*, 2002, **487**, 612.
19 P. Kirkegaard, M. Eldrup, O. E. Mogensen and N. J. Pedersen, *Comput. Phys. Commun.*, 1981, **23**, 307–335.
20 G. A. Bottomley, I. J. Clark, I. I. Creaser, L. M. Engelhardt, R. J. Geue, K. S. Hagen, J. M. Harowfield, G. A. Lawrance, P. A. Lay, A. M.

Sargeson, A. J. See, B. W. Skelton, A. H. White and F. R. Wilner, *Aust. J. Chem.*, 1994, **47**, 143.
21 N. M. Di Bartolo, A. M. Sargeson, T. M. Donlevy and S. V. Smith, *J. Chem. Soc., Dalton Trans.*, 2001, 2303.
22 Unpublished data.
23 D. W. Gidley, W. E. Frieze, T. L. Dull, J. Sun, A. F. Yee, C. V. Nguyen and D. Y. Yoon, *Appl. Phys. Lett.*, 2000, **76**, 1284.
24 S. V. Smith, *Q. J. Nucl. Med. & Mol. Imag.*, 2008, **52**(2), 193.
25 S. V. Smith, *J. Inorg. Biochem.*, 2004, **98**, 1874and reference within.
26 S. Chaves, R. Delgado, J. J. R. Frausto and Da Silva, *Talanta*, 1992, **39**, 249.
27 E. T. Clarke and A. E. Martell, *Inorg. Chim. Acta*, 1991, **190**, 27.
28 A. E. Martell, R. M. Smith, *Critical Stability Constants*, vol. 62nd Supplement, Plenum Press, New York, 1989.
29 L. Grøndahl, A. Hammershøi, A. M. Sargeson and V. Thom, *Inorg. Chem.*, 1997, **36**, 5396.
30 M. Pourbaix, in *Atlas of Electrochemical Equilibria in Aqueous Solutions*, NACE, Texas, 1974.

